Extended Abstract DOI: https://doi.org/10.64862/ajeg.2025.2sp.42.145 Open Access

Quantitative Analysis of Greening for Sustainable City

Sultana Nasrin Nury[1*], Jason Beringer[2], Nigel Tapper[3] and Andrew Coutts[3]

[1]Geological Survey of Bangladesh, Segunbagicha, Dhaka, Bangladesh
[2]The University of Western Australia, Crawley, Australia
[3]Monash University, Melbourne, Australia

(*Corresponding E-mail: nurysn@yahoo.com)

Received: September 20, 2025, Accepted: October 17, 2025

Abstract: This study quantitatively analyses the spatial relationship between land surface cover and urban surface temperature distribution among different land use classes in metropolitan Melbourne. This relationship was explored through a detailed estimate of fractional land cover at 30 m grid resolution using LiDAR data along with land surface temperature (LST) and modeled heat fluxes using Landsat TM5 data. In this study spatially distributed energy fluxes specifically ET, in an urban area were modeled based on an energy balance approach incorporating the surface roughness parameters derived from the LiDAR Data. This study shows a strong and significant linear relationship between LST and the percentage of different types of land cover. The relationship is positive for built-up areas and negative for vegetated areas. Such relationship quantitively depicts that with increasing total vegetation cover the LST decreases; in contrast LST increases linearly with increased imperviousness.

Keywords: ***LST, ET, Landsat TM5, LiDAR, Energy balance modeling.***

Introduction

A sustainable city endures the social, environmental and economic stresses and performs as a resilient habitat for the existing and future generation through prudent urban planning and city management. Urbanization transforms the natural lands into built-up areas which create complex and heterogeneous land surface properties. Urban air temperature is strongly influenced by the built environment and is significantly warmer than its surrounding rural or peri-urban areas. To reduce the thermal impact and to achieve human thermal comfort several studies suggest the addition of green space and vegetation as an important heat mitigation option (Coutts et al., 2013). Green surfaces use available energy and water for evapotranspiration (λ_{ET}) therefore less energy is available for atmospheric heating (H) and heat storage (G), which resulted a cooler urban environment. However, such planning requires detailed information about the land surface heterogeneity and spatial relations between land surface covers and surface energy fluxes in different land use classes (Coutts et al., 2013; Grimmond, 2007). With its synoptic capability, satellite images retrieve this information rapidly and economically. Recent development of LiDAR data offers highly detailed land cover information in an urban area and along with height information of urban elements.

Three local government areas (LGA) namely Melbourne, Monash and Darebin LGA of metropolitan Melbourne were selected for this study (Figure 1). Each of the LGA is different in characteristics such as settlement age, geology, geographical setting, population density, land use, business types, and other attributes.

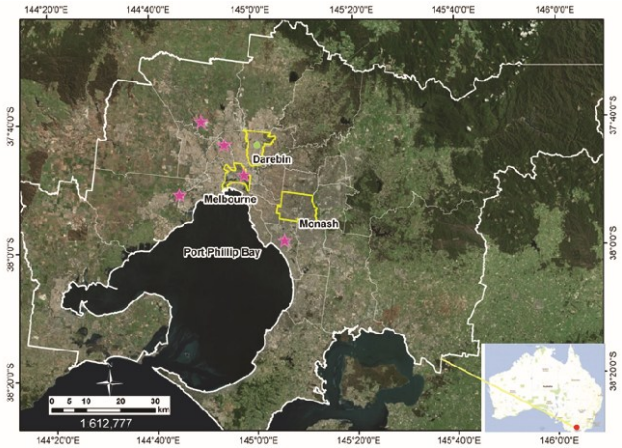

Figure 1, Location map of the study area. The magenta dots indicate weather stations, and the green dot represents energy flux monitoring tower.

Methodology

Detailed land cover extraction from LiDAR data

In this study, classified LiDAR data according to the LAS 1.2 specification code has been used to generate a detailed land cover map at sub-meter resolution using geospatial tool of ArcGIS. Six types of land cover information were extracted for each LGA and these datasets included: 1) building, 2) road, 3) trees, 4) grass, 5) other impervious area and 6) water. Other impervious areas include parking, courtyards or dry, bare soil.

Table 1, Percentage of area covered by different land cover types in three city council areas.

Name of the city council	Percentage (%) of land cover type					
	Building area	Road area	Impervious area	Tree crown area	Grass	Water

Melbourne	21.8	15.4	32.1	9.9	14.8	6
Monash	19.5	15.4	14.6	24	26	0.4
Darebin	25.2	16.7	13.4	12.8	31.1	0.8

Fractional land covers estimation

Detailed land cover maps were derived from very high-resolution LiDAR data. In absence of very high-resolution spatial temperature data, estimation of surface temperature and surface heat fluxes were derived from medium 30-meter resolution Landsat data. At the ground, these 30 m-by-30m land areas could include several different types of cover. The reflectance that the satellite sensor receives is a mixture of reflectance from different land covers for each pixel. To overcome the challenge, land cover fractions at a 30 m grid scale were derived to estimate the relationship between land cover types with other satellite-derived parameters (Figure 2). A regular 30 m by 30 m vector grid was created for this purpose and within this 30 m grid, the fraction of each land cover type was calculated using the Statistical tool of ArcGIS. Each of these grids has an individual identification number (ID no).

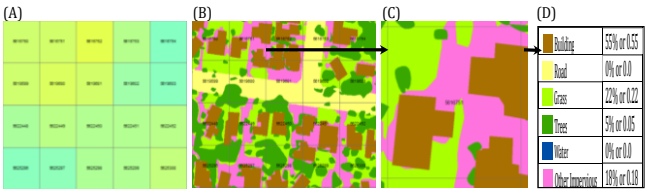

Figure 2, A) The black lines represent a regular 30m by 30m vector grid derived from Landsat Tm Raster with their ID no., (B) The derived detailed land cover map from the LiDAR data is overlain on the 30m by 30m vector grid, (C) Enlarged view of an individual 30 m grid and (D) the contained land cover fraction of an individual grid.

For each building and tree polygon, the mean elevation was extracted from LiDAR data considering flat rooftop for building and smooth canopy for vegetation. Mean building height and tree height for each grid were calculated using the following equation (Burian et al., 2004),

$$\bar{h} = \frac{\sum_{i=1}^{N} h_i}{N} \text{ and } S_h = \sqrt{\frac{\sum_{i=1}^{N}(h_i - \bar{h})^2}{N-1}} \quad \text{.....(1)}$$

where, h is the mean elements height of N number of elements for each grid, S_h is the standard deviation of building height, h_i is the height of building i and N is the total number of buildings in the area. Using the same equation, mean tree height was also derived for each grid. The displacement height (Z_d) and roughness length (Z_o) are the key parameters used in energy balance model to specify the boundary conditions above built-up areas. These two parameters were calculated following Grimmond and Oke (1999) are

$$Z_d = \int_d \overline{Z_H} \text{ and } Z_o = \int_0 \overline{Z_H} \quad \text{.....(2)}$$

where, Z_H is the average building height and ∫d and ∫0 are empirical coefficients. Grimmond and Oke (1999) assumes 0.5 for ∫d and 0.1 for ∫0 in urban areas.

The surface brightness temperature (T_{bb})

It was computed from spectral radiance in band 6 by the following Markham and Barker, 1986 using Landsat TM5 data (93/86 row/path dated 14-10-1989, 03-09-2003, 01-04-2005, 12-09-2006, 24-12-2003, 24-11-2004, 01-11-2005 and 28-02-2005).

$$T_{bb} = \frac{K_2}{ln\left(\frac{K_1}{L_6}+1\right)} \quad \text{..... (3)}$$

where, L_6 is the spectral radiance at sensor of the thermal band (band 6); T_{bb} is effective at-satellite surface brightness temperature and $K_1$and $K_2$are constants for Landsat TM. The surface temperature (T_s) was then computed according to Liu et al., (2007).

$$T_s = \frac{T_{bb}}{(\varepsilon_O)^{0.25}} \quad \text{..... (4)}$$

where, ε_O is surface emissivity. Following Griend (1991) $\varepsilon_O$was estimated using NDVI.

Surface heat flux modeling

According to Oke (1988) the surface energy balance can be explained as the total incoming solar net radiation R_n (W/m²) is divided in to the sensible heat flux H (W/m²) that warm the air, λ_{ET} (W/m²) the latent heat flux which is used for evapotranspiration, G (W/m²) is the storage heat flux which is stored within the urban fabric and canopy layer. In this study anthropogenic heat component was not considered.

$$R_n = G + H + \lambda_{ET} \quad \text{..... (5)}$$

The net surface radiation (R_n) at the satellite overpass time was computed from Landsat TM5 data following Allen et al., (2007) and Bastiaanssen et al., (1998).

$$R_n = R_s - \alpha R_{s(in)} + R_{L(in)} - R_{L(out)} - (1-\varepsilon_0)R_L \text{ ... (6)}$$

where, R_s (in) is the incoming short-wave radiation, α is the surface albedo (dimensionless), R_L (in) is the incoming long-wave radiation, R_L (out) is the outgoing long-wave radiation, ε_0 is the broadband surface thermal emissivity. The term $(1-\varepsilon_0)R_L$ represents the fraction of incoming long-wave radiation reflected from the surface. The G is estimated according to Liu et al., (2010) using surface temperature, albedo, and normalized difference vegetation index (NDVI).

$$G = R_n[(T_s - 275.15) \times (0.0038 + 0.0074\alpha) \times (1 - 0.98NDVI^4)$$
..... (7)

where, R_n is total radiation and α is surface albedo, Ts is surface temperature (in Kelvin). H is computed using the following equation (Bastiaanssen et al., 1998)

$$H = \frac{(\rho \times C_p \times dT)}{r_{ah}} \quad \text{..... .... (8)}$$

where, ρ is air density (kg m-3), C_p is air specific heat, d_T is the temperature difference and r_{ah} is the aerodynamic resistance. Λ_{ET} for the time of the satellite

overpass is computed at each pixel as residual of the energy balance using the following equation (Bastiaanssen et al., 1998a):

$$\lambda_{ET} = R_n - G - H \text{ and } ET_{inst} = 3600\frac{\lambda_{ET}}{\lambda} \ldots\ldots\ldots (9)$$

The instantaneous ET (ET_{inst}, mm/hr.) is defined as the evapotranspiration at the time of the satellite overpass and λ is the latent heat of vaporization.

Results

Statistical analysis shows that with a 10% increase in impervious cover, the LST increases about 0.6°C to 1.3°C during summer and about 0.38°C to 0.76°C in winter. On the other hand, for each 10% increment of tree areas, the LST decreases about 1.0°C to 0.7°C during summer and about 0.56°C to 0.33°C during winter in Melbourne. These values are much lower for grass cover. For example, each 10% increment of grass decreases the LST of about 0.27°C to 0.54°C in summer and 0.13°C to 0.28°C in winter (Figure 3).

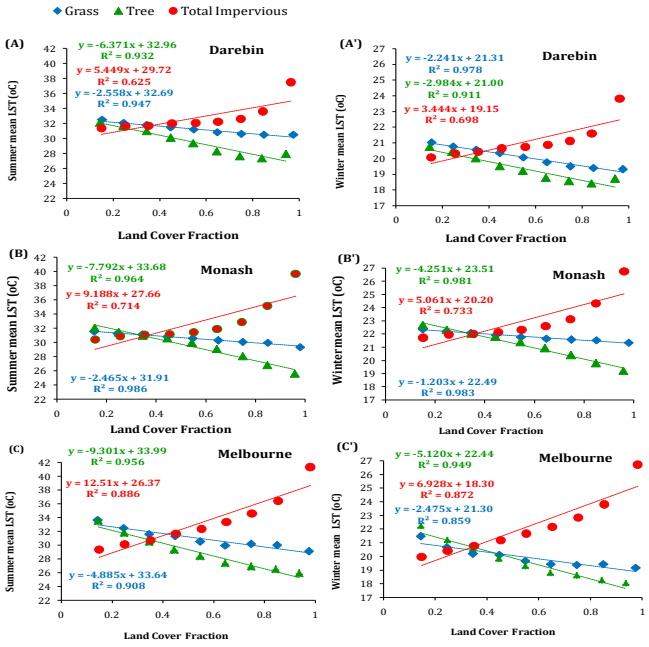

Figure 3, Relationship between summer LST and land cover of three LGAs.

The estimated energy fluxes showed significant effect due to spatial land cover variability. Impervious cover was the dominating factor for the spatial distribution of G and H. In all three LGAs, the value of G increased with increasing impervious cover and decreased with increasing vegetation cover, but the effect is more evident for trees than for grass cover. In all three study areas, the spatial distribution of H was highly variable. The ET rate also varies significantly for grass and trees. Grass cover always showed higher mean LST even when it had higher mean ET values (Figure 4).

The LST and ET were inversely correlated for both grass and trees, and the coefficient of determination (R2) is more than 0.9 for trees in all three areas, whereas for grass it is more variable and ranges from 0.2 to 0.9. From the statistical analysis it is evident that increases in ET rate and associated decreases in LST are higher for trees than grass, indicating that trees are more efficient than grass for LST reduction in the urban environment of Melbourne. As LST has a direct influence on air temperature, trees will be most effective to reduce air temperature and mitigate excess urban heat.

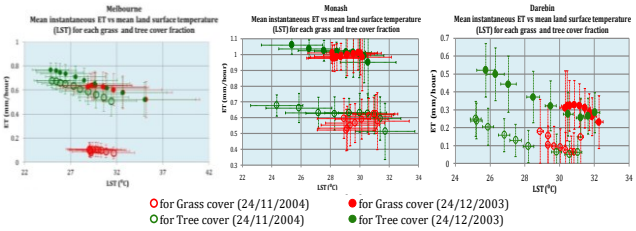

Figure 4, Relationships between surface temperature and ET_{inst} rates for tree and grass cover for the three city councils.

Conclusions

This study demonstrates that remote sensing data can be used as a tool for informed implementation of greening as a heat mitigation measure in an urban area to achieve a sustainable city. The resulting relationships can also facilitate the planning of a balanced spatial arrangement of land use types where areas prone to excessive heat can be managed into relatively cooler land uses.

Acknowledgement

This paper is an output of PhD research. The first author sincerely acknowledges Monash University, Melbourne, Australia for funding and the Geological Survey of Bangladesh for the permission to undertake this research in Australia.

References

Allen, R. G., Tasumi, M., Morse, A., Trezza, R., Wright, J. L., Bastiaanssen, W., Kramber, W., Lorite, I., and Robison, C. W. (2007). Satellite-based energy balance for mapping evapotranspiration with internalized calibration (METRIC)-Applications. Journal of Irrigation and Drainage Engineering, 133 (4), 395–406. https://doi.org/10.1061/(ASCE)0733-9437(2007)133:4(395)

Bastiaanssen, W. G. M., Menenti, M., Feddes, R. A., and Holtslag, A. A. M. (1998). A remote sensing surface energy balance algorithm for land (SEBAL): 1. Formulation. Journal of Hydrology, 212–213, 198–212. https://doi.org/10.1016/S0022-1694(98)00253-4

Burian, S. J., Stetson, S. W., Han, W., Ching, J., and Byun, D. (2004). High-resolution dataset of urban canopy parameters for Houston, Texas. In Proceedings of the 5th Symposium on the Urban Environment, Vancouver, BC, Canada (Paper 9.3).

American Meteorological Society. Available at: https://www.researchgate.net/publication/228931671_High-resolution_dataset_of_urban_canopy_parameters_for_Houston_Texas

Coutts, A. M., Tapper, N. J., Beringer, J., Loughnan, M., and Demuzere, M. (2013). Watering our cities: The capacity for water sensitive urban design to support urban cooling and improve human thermal comfort in the Australian context. Progress in Physical Geography, 37(1), 2–28. https://doi.org/10.1177/0309133312461032

Grimmond, S. (2007). Urbanization and global environmental change: Local effects of urban warming. Geographical Journal, 173(1), 83–88. https://doi.org/10.1111/j.1475-4959.2007.232_3.x

Grimmond, C. S. B., and Oke, T. R. (1999). Evapotranspiration rates in urban areas. In Impacts of Urban Growth on Surface Water and Groundwater Quality (IAHS Publication No. 259, pp. 235–243). International Association of Hydrological Sciences. Available at: https://iahs.info/uploads/dms/11465.235-243-259-Grimmond.pdf

Liu, S., Hu, G., Lu, L., and Mao, D. (2007). Estimation of regional evapotranspiration by TM/ETM data over heterogeneous surfaces. Photogrammetric Engineering and Remote Sensing, 73(10), 1169–1178. https://doi.org/10.14358/PERS.73.10.1169

Liu, W., Hong, Y., Khan, S. I., Huang, M., Vieux, B., Caliskan, S., and Grout, T. (2010). Actual evapotranspiration estimation for different land use and land cover in urban regions using Landsat 5 data. Journal of Applied Remote Sensing, 4(1), 1-14. https://doi.org/10.1117/1.3525566

Markham, B. L., and Barker, J. L. (1986). Landsat MSS and TM post-calibration dynamic ranges, exoatmospheric reflectances and at-satellite temperatures. Earth Observation Satellite Company.

Oke, T. R. (1988). The urban energy balance. Progress in Physical Geography, 12(4), 471–508. https://doi.org/10.1177/030913338801200401